Design and implementation of an air flow measurement extension for a wood pellet water heater

HAMK
HÄMEEN AMMATTIKORKEAKOULU
HÄME UNIVERSITY OF APPLIED SCIENCES

Bachelor's thesis

Häme University of Applied Sciences
Valkeakoski campus
Electrical and Automation Engineering

Spring 2020

Ivan Khvorostin

HAMK
HÄMEEN AMMATTIKORKEAKOULU
HÄME UNIVERSITY OF APPLIED SCIENCES

ABSTRACT

Electrical and Automation Engineering
Valkeakoski campus

Author Ivan Khvorostin **Year** 2020

Subject Design and implementation of an air flow measurement extension for a wood pellet water heater

Supervisor(s) Katariina Penttilä

ABSTRACT

The goal of the thesis project was to design and implement an airflow measurement solution for the VEneCT project. Computer simulation and mathematical modelling of the process were used to determine the best flow properties which were verified by experiment. Another goal was approving the hypothesis that smaller cost-efficient sensors are suitable for measuring the airflow in bigger size pipes using the bypass configuration.

The following activities were accomplished during the thesis project work: Fundamental theoretical research of airflow principles and airflow measurements with cost-efficient MEMS (Micro-Electro-Mechanical Systems).

Flow measurement extensions were designed as addition to the existing air flow system with Autodesk Invertor software and the expected air flow was simulated in the CFD (Computational Fluid Dynamics) simulation software, Autodesk CFD.

Testing the simulated results was conducted on the prototype modelling and creating a mathematical model based on the test results using the nonlinear regression analysis method to find the connection between the sensor's output and the real flow in the main channel. As a conclusion a verification of the interactions between the simulating results, experimental results and mathematical model.

Simulation with the modern CFD software is an effective and cost-efficient method for designing an optimal model for flow measurement. The use of the CFD significantly reduces the prototyping stage of a research project and saves on resources. A mathematically determined function based on both simulating data and experimental results provides an accurate concept of the flow process and was implemented to the flow control software of VEneCT. The measurement is possible with only 7 % error. Properly calibrated MEMS is a reliable method to measure an airflow when used in bypass configuration and tested to match the desired measurement environment.

Keywords Calibration, CFD, MEMS, venturi tube, VEneCT
Pages 26 pages including appendices 3 pages

CONTENTS

LIST OF FIGURES

LIST OF TABLES

ABBREVIATIONS AND SYMBOLS USED

CFD	computational fluid dynamics
CNC	computer numerical control
DMM	digital multimeter
K	Kelvin
L/min	liters per minute
l/s	liters per second
m	meters
m^3/h	cubic meter per hour
m^2	square meters
m/s	meters per second
MEMS	micro electro-mechanical system
Micro-CHP	micro combined heat and power
nm	nanometers
PLC	programmable logic controller
V	colt
W	watts

1 INTRODUCTION

Digital and technological revolution have created new opportunities for process automation and measurement applications. The complexity and precision of processes have increased significantly during the past years. At the same time, the size of electronics components, for example microprocessors, has decreased from 10 000 nm to 16 nm or 625 times, during forty years (Gruener & Miconi, 2018). Measurement in modern processes requires complex and expensive instrumentation that utilizes both fundamental physical principles and advanced micro-electronic technologies. In these circumstances, MEMS instrumentation is the best solution. Digitalization allows us to use perfectional-grade software even for small application. CFD software brings such level of design and process simulations solutions that previously was available only in industrial-grade applications.

Global Micro-Electro-Mechanical Systems market reached USD 11.6 billion in 2018 and is expected to grow by 8.2 percent up to 2024 (Dahad & Pele, 2019). Because of mass production, the manufacturing process of a MEMS requires less resources and raw materials, contributes to the modern trend of sustainable manufacturing.

Flow measurement is one of the most common tasks in many processes. There are multiple ways and principles to measure the flow rate. Measuring principle is normally selected based on multiple factors, such as the type of the measured substance, properties and characteristics of the process, the temperature, humidity level and many others.

In this thesis, the process of air flow measurement extension design, sensor calibration and mathematical function determination will be presented. MEMS technology and CFD modeling were utilized to create innovation approach to solve problems.

Mathematical modeling and statistical method where used to calculate equation for volumetric flow value as function of sensor output voltage. Such an equation will be used for the installed sensor to provide real time values of air flow inside of the air duct.

The main thesis hypothesis is that the MEMS installed in the bypass configuration with specifically designed extension, and properly calibrated, is suitable for measuring air flow, and that even the slightest change in the flow to both directions can be detected and measured.

The thesis project work was conducted with a pellet burner installed on HAMK VEneCT project site in Valkeakoski, Finland. The burner is equipped with a primary air delivery fan, but there is neither measurement devices for volumetric flow rate measurement nor the output signal for connecting

flow measurement device to control unit. Such a measurement solution is necessary for achieving the goals of the main VEneCT project: the optimization of the burning process and converting the water heating station to a Micro-CHP plant. The commissioning party of the thesis project is HAMK Tech research unit.

Micro-CHP uses wood pellets as a burning material to heat up the water. The combustion process requires fuel, heat and oxygen to continue. The amount of oxygen available in the system is a critical part of the combustion process. Knowing that parameter is necessary to determine the efficiency of the combustion process.

The first challenge when designing the air flow measurement solution for the small pellet burner was the selection of suitable flow measurement instrument. As mentioned earlier, there are multiple ways to measure the air flow rate available on the market. Industrial grade sensors are commonly used to measure the air flow in the large-scale processes, and it is a reliable way to do so. But for a smaller process such an instrument will have several limitations, such as high initial price and complex installation. In addition, larger instruments are made to measure the flow in large diameter pipes. MEMS are smaller and easier to install than industrial grade instruments. MEMS sensors are more cost efficient and provide relatively high resolution and sensitivity.

The second problem was to design the sensor installation point to fit in the very limited space available in the boiler room. At the same time, the instrument installation point will have to create minimum turbulence in the flow. In addition, the instrument must be reliable and easy to install.

The third challenge was to determine the connection between the sensor's output signal and the actual flow in the air duct. The connection was expressed with mathematical equation, and the equation will be used in PLC code for process controlling purpose.

To solve all listed problems, the following was proposed in this thesis work:

- Use of the Omron® d6f-ph0025ad1 MEMS Flow Sensor, installed in the bypass configuration, as the main instrument for flow measurement.
- Design of the venturi flow restrictor to create enough pressure drop for sensor's operation and at the same time ensure minimum turbulence in the flow created by the restrictor.
- The design was tested with the Autodesk ® CFD software for best result.
- The airflow velocity was experimentally determined for all available ranges of the airflow.
- Turbulence was analyzed experimentally with CFD software in all range of air velocities to determine that measurement requirements are met.

– The prototypes of the sensor extension tubes were 3D printed and tested. The final model was 3D printed and installed in the process.

2 THEORETICAL BASIS OF AIR FLOW EXTENSION DESIGN

2.1 Operating principles of D6F-P sensor

D6F-P sensors are used in many applications where low flow rate is presented and very small changes of it will have to be detected. D6f-ph0025ad1 sensor has a temperature distribution heater element that is heated symmetrically when there is no flow. When flow is presented, the temperature of the upstream side cools down and the temperature of the downstream side warms up, disrupting the symmetry of the temperature distribution, as illustrated in Fig 1. By detecting the temperature difference as a difference of the electromotive forces developed by thermopiles, the flow rate can be determined without influence of temperature of pressure from the environment.

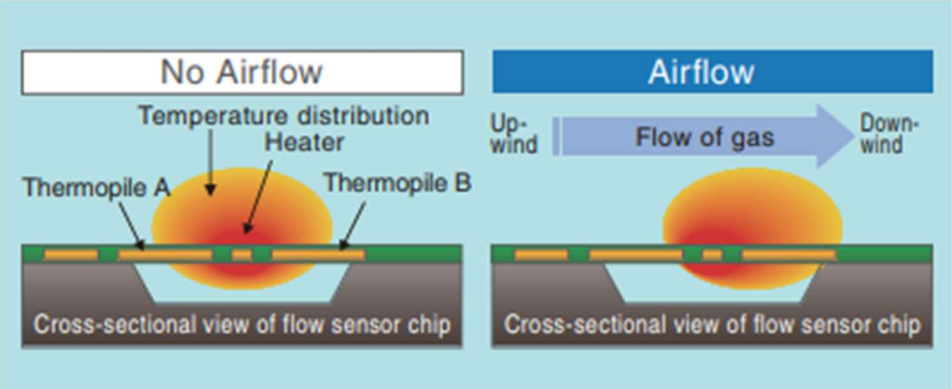

Figure 1. D6F sensor operation (Sensors Selector Guide, 2018)

A DF6 sensor has a relatively high duct resistance. The patented technology utilizes centrifugal separation to ensure a minimum level of the dust particles presented to the sensor. (Sensors Selector Guide, 2018)

The sensor is factory calibrated to measure clean air and outputs the analog signal as a voltage from 0.5 V to 2.5 V. It has four calibrated points representing the Flow rate as L/min as illustrated in Fig 2.

D6F-P0010A1/-P0010A2/-P0010AM2

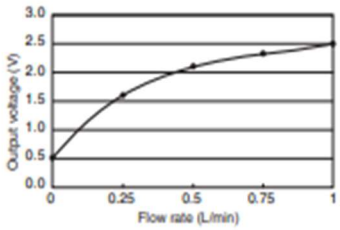

Flow rate L/min (normal)	0	0.25	0.50	0.75	1.00
Output voltage V	0.50 ±0.10	1.60 ±0.10	2.10 ±0.10	2.31 ±0.10	2.50 ±0.10

Measurement conditions: Power supply voltage of 5.0±0.1 VDC, ambient temperature of 25±5°C, and ambient humidity of 35% to 75%.

Figure 2. Factory calibrating data (MEMS Flow Sensors catalog, 2006)

2.2 **Regression analysis**

Regression analysis is used to describe the dependence between one dependent and one or more independent variables. As a result of the regression analysis, a mathematical function was created. The regression model describes the functional dependence between the dependent and independent variable. Regression model should describe the observed data as well as possible. Predicted values, given by the model, should be as close to observed data as possible.

In linear regression, the objective is to find equation 1 of straight line so that the error between the observed data (yi, xi) and the points in the line is as small as possible.

$$y = f(x) = ax + b \tag{1}$$

To minimize the errors the equation 2 was used:

$$\varepsilon i = yi - f\ xi$$
$$\varepsilon i = yi - axi + b$$
$$\varepsilon i = yi - axi - b$$
$$\text{f(a, b)} = \sum_{i=1}^{n} \varepsilon^2 = \sum_{i=1}^{n} (\text{yi} - \text{axi} - \text{b})^2 \tag{2}$$

Extrema's of the function can be determined by using the gradient method that is illustrated in equation 3.

$$\begin{cases} -2\sum_{i=1}^{n} x_i(y_i - ax_i - b) = 0 \\ -2\sum_{i=1}^{n} (y_i - ax_i - b) = 0 \end{cases}$$

$$a\sum_{i=1}^{n} x_i^2 + b\sum_{i=1}^{n} x_i = \sum_{i=1}^{n} x_i y_i$$

$$a\sum_{i=1}^{n} x_i + nb = \sum_{i=1}^{n} y_i$$

$$\nabla f\ a, b = 0 \Leftrightarrow \begin{matrix} \partial f\ (a, b)\ \partial a = 0 \\ \partial f\ (a, b)\ \partial b = 0 \end{matrix}$$

(3)

When rewriting equation 3, we will find the smallest values for coefficients a and b. The result is illustrated by equation 4. Values from equation 4 will be substituted to equation 3 and gradient was found.

(4)

$$a = \frac{n\sum_{i=1}^{n} x_i y_i - [\sum_{i=1}^{n} x_i] \cdot [\sum_{i=1}^{n} y_i]}{n\sum_{i=1}^{n} x_i^2 - [\sum_{i=1}^{n} x_i]^2}$$

$$b = \frac{[\sum_{i=1}^{n} x_i^2] \cdot [\sum_{i=1}^{n} y_i] - [\sum_{i=1}^{n} x_i] \cdot [\sum_{i=1}^{n} x_i y_i]}{n\sum_{i=1}^{n} x_i^2 - [\sum_{i=1}^{n} x_i]^2}$$

For regression model testing, two methods were used: residual analyses of the regression model and least-squares test.

Residuals are the variations between the one-step predicted output of the models and the measured output from the test data set. Thus, residuals are part of the verification data not explained by the model. In this project, the sensor's output was compared to different model fittings in order to find the optimal mathematical representation of the process. The method of the analysis was taken from the MathWorks website knowledge database. (What Is Residual Analysis?, n.d.)

Residual analysis consists of two tests: the whiteness test and the independence test.

According to the whiteness test criteria, a proper model has the residual autocorrelation function within the confidence interval of the corresponding assessments, indicating that the residuals are uncorrelated.

According to the independence test criteria, a decent model has residuals uncorrelated with measured responses. Indication of correlation shows that the model does not define how a section of the output correlates to the corresponding input.

2.3 Statistical and mathematical methods for error evaluation.

The standard deviation method described by equation 5 was used to determine the deviation of the measured values from the model values. The expected value was determined from the regression function after an experiment.

$$\sigma = \sqrt{\frac{\sum_{i=1}^{n} (x_i - \bar{x})^2}{n-1}} \tag{5}$$

where:

$\bar{x}$= samples mean;
n- samples size;

A graphical analysis and coefficient of determination was used in addition to the deviation determination. Relative error method, generally described by equation (6), will be used to determine measurement error, or in other words - accuracy of the flow measurement.

$$\text{relative Error: } \frac{\text{Deviation}}{\text{measured quantity}} \tag{6}$$

Total deferential method for error propagation was used to evaluate the final model equation. The exact formula for propagation of error is equation 7. The equation 7 will be modified to solve error of final model.

$$\Delta f = \frac{\partial f}{\partial x} dx + \frac{\partial f}{\partial y} dy + \frac{\partial f}{\partial z} dz \tag{7}$$

2.4 Velocity measurement in the rectangular shape air duct

The principle and methodology of the air flow measurement is specified in ISO 3966 standard (ISO 3966:2008 Measurement of fluid flow in closed conduits, 2008). The method described in the ISO 3966 also known as the

Log-Tchebycheff method. The standard specified that 25 measurement points for a rectangular duct will have to be selected and 30 diameters from the disturbance in the rectangular shape duct will have to be held for measurement uncertainty of 3 % of the flow rate. In practice it is not always possible to follow the exact recommendations that's why flow properties and measurement uncertainty was found experimentally and confirmed with CFD simulation.

Differences from the recommended by Log-Tchebycheff method values dictated by the physical limitation of the process. It is not possible to take measurements at the distance of 30 diameters from disturbance because of limited available space at the process site. To compensate disturbance effect on the flow, CFD modeling was used. Another difference was that measurement uncertainty can no longer be assumed to be 3% and must be reevaluated. Detailed step by step implementation of the Log-Tchebycheff method was described in chapter 3.3.1 of this thesis. Measurement uncertainty was evaluated in chapter 4.1 of this thesis.

2.5 **CFD analyses**

Before the experiment begins, several important properties of the measured substance must be determined in order to use correct methodology for flow measurement. In the experiments and later in the actual process the air is at a temperature range between 283 and 333 K. The maximum measured air velocity that the air blower can provide does not exceed ten m/s. The air is relatively clean from particles and the sensor is equipped with a particle filtering system as described in chapter 2.1. Summarizing all data, one can assume that in the experiment there will be compressible, turbulent, unsteady, subsonic air flow to measure.

The fundamental basis behind the flow measurement and venturi flow restrictor design is Bernoulli's, illustrated by equation 8.

$$p_1 + \rho g h_1 + \frac{1}{2} C p v_1^2 + \Delta p_p = p_2 + \rho g h_2 + \frac{1}{2} C p v_2^2 + \Delta p_l \qquad (8)$$

Where:

p_1, p_2 : pressure.
v_1, v_2 : velocity of fluid.
h_1, h_2 : height.
ρ_1, ρ_2 : density of fluid.
C: flow coefficient. In our case 2 for turbulent flow
Δp_P : the pressure difference generated by the blower.
Δp_l : all the pressure losses caused by losses caused by pipes, bends, valves etc.

Equation 8 takes in to account the presence of turbulence, wall friction and pipe bends. In a real application the error or the numerical calculation would be significant if only the equation method was used. The air that will

be delivered to the process will be of various temperatures and different velocities. Combination of these factors makes manual numerical evaluation very complex and subject to error. Considering that the sensor was mounted on flexible tubes and the fan was blowing a relatively turbulent flow from the very beginning, another method to study the flow properties was considered. CFD - Computational fluid dynamics was selected as more convenient to ensure high accuracy of the design.

CFD is subsection of continuum mechanics, including a set of physical, mathematical and numerical methods was designed to calculate the characteristics of stream processes. In this thesis, the physical and numerical methods was mainly used to find the most optimal shape for the sensor extension point design.

3 PLANNING AND IMPLEMENTATING MEASUREMENT EXTENSION

3.1 Air duct design process

The air to the process is delivered with the AC centrifugal fan, with a maximum output flow of 281 m^3/h . The output portal of the fan was directly connected to the air intake of the process, and it has rectangular shape. In order to place the flow sensor, the extension tube with venture flow resistor must be designed and installed to be located between the fan and the intake portal. The extension has 3 parts, which have been tested for flow turbulence separately and as connected unit at Autodesk CFD 2019.

Experiment for turbulence determination consisted of following steps:
Step one was the air velocity measurement at the end of the extension, following method described by ISO 3966:2008 (ISO 3966:2008 Measurement of fluid flow in closed conduits, 2008). The testing station is illustrated on the Fig 3.

Figure 3. Testing station for log-Tchebycheff method

The second step was to simulate the airflow with the CFD software to verify the experimental data. The third step was to examine the data of the experiments to determine the acceptable for flow measurement level of turbulence.

3.2 **Air duct design**

The air duct extension consists of three parts. The upper and lower parts were made to create a transition between the rectangular and circular structures of the fan's portal and the venturi tube. The drawing of the parts is illustrated in Fig 4. The length of the parts, 109 mm, was determined by using Autodesk CFD simulation software to ensure a low turbulence for the intake and output of the sensor extension.

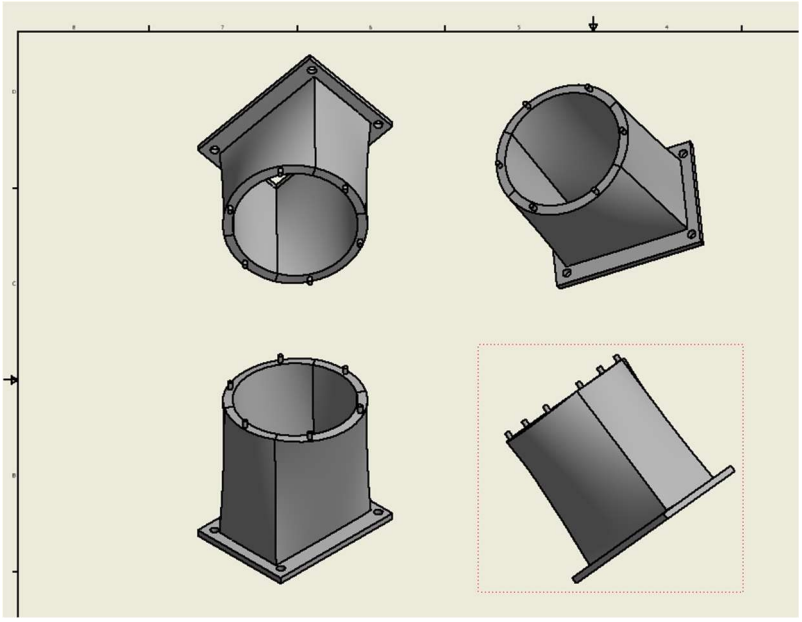

Figure 4. Upper and lower parts of the air duct extension

The middle part of the extension is a venturi flow restrictor. It was designed and tested with CFD software, as illustrated in Fig 5. The flow is relatively laminar and does not have major turbulences presented.

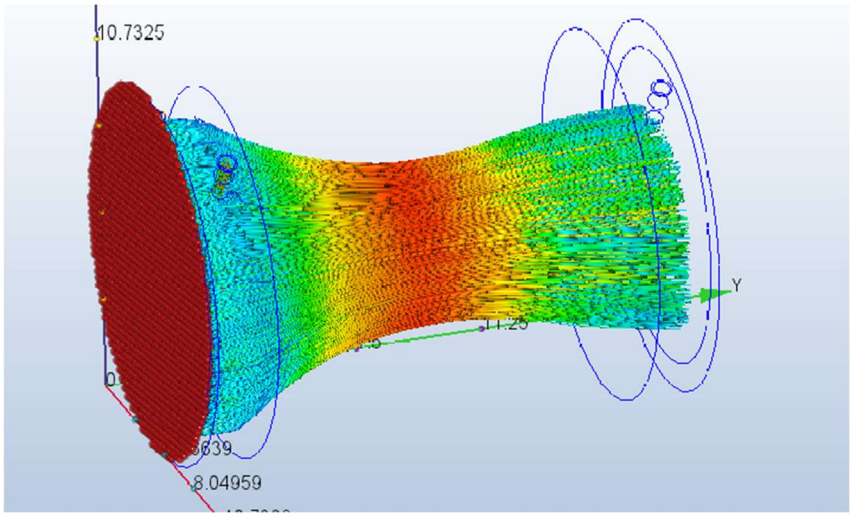

Figure 5. Venturi flow restrictor. CFD simulation results

A venturi flow restrictor was designed as to ISO 5167-1:2003 (ISO 5167-4:2003 Measurement of fluid flow by means of pressure differential devices inserted in circular cross-section conduits running full — Part 4: Venturi tubes, 2003). It was created symmetrical in order to be able to detect a reverse flow, if any will take place. Final drawing of the flow restrictor is shown in Fig 6.

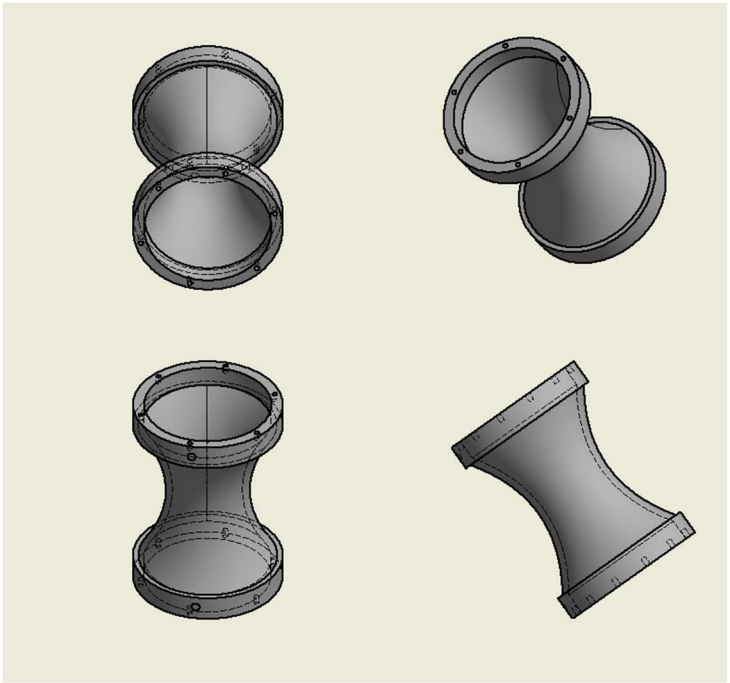

Figure 6. Venturi flow restrictor drawing

As it was mentioned in chapter 2.1, the D6F-P sensor is a volume flow sensor that works at a range from 0 to 1 L/s. The sensor was attached to the venturi extension with soft PVC tubes 153 mm in length and 4 mm in inner diameter, as recommended in the sensor's datasheet (MEMS Flow Sensors catalog, 2006). Printed testing exertion is illustrated in Fig 7.

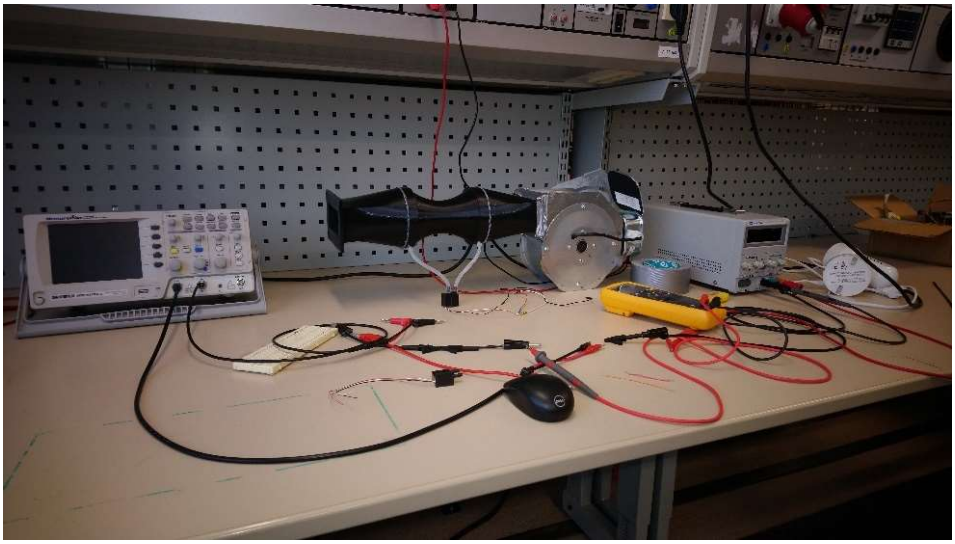

Figure 7. Calibrating station

In the experiment, the sensor was installed in a bypass configuration, with the only portion of the flow passing through it. The bypass configuration allows one to measure a much greater flow up to 200L/s (MEMS Flow Sensors catalog, 2006). In this way it is possible to use all the advantages of the sensor type. The estimated flow through the sensor was determined with CFD software by running the flow simulation, and the diameter of the venturi tube was adjusted in order to insure an optimal bypass flow ratio.

The sensor's ports were 4.9 mm in diameter. The inner diameter of the venturi tube was 50 mm and the main channel diameter is 93 mm. The optimal ratio close 1/2 between the main tube diameter and middle diameter of the venturi tube was determined with the CFD simulation to create the significant pressure drop and minimum turbulence. With that ratio it was possible to utilize the sensor's range and at the same time the bypass flow did not exceed the sensors maximums.

In order to confirm an acceptable turbulence level created by the venturi flow resistor, separate tests were made for flow consistency using a velocity sensor following the methodology of the ISO 3966 standard (ISO 3966:2008 Measurement of fluid flow in closed conduits, 2008). The testing setup is illustrated in Fig 8. In addition to ISO 3966, the method was described in an article (TSI Instruments Ltd, 2014). Both sources were used for better accuracy of the results.

Figure 8. Venturi turbulence test station

3.3 **Sensor calibration**

3.3.1 Methodology

The calibration was accomplished according to the instructions in the ISO 3966:2008 standard (ISO 3966:2008 Measurement of fluid flow in closed conduits, 2008). A few necessary adaptations were made in order to adjust the calibration process.

The air duct was divided into rectangular areas adjusted in size as specified in ISO 3966:2008. The flow velocity at 30 points inside the duct was measured in order to get a good average value, as illustrated in Fig 9.

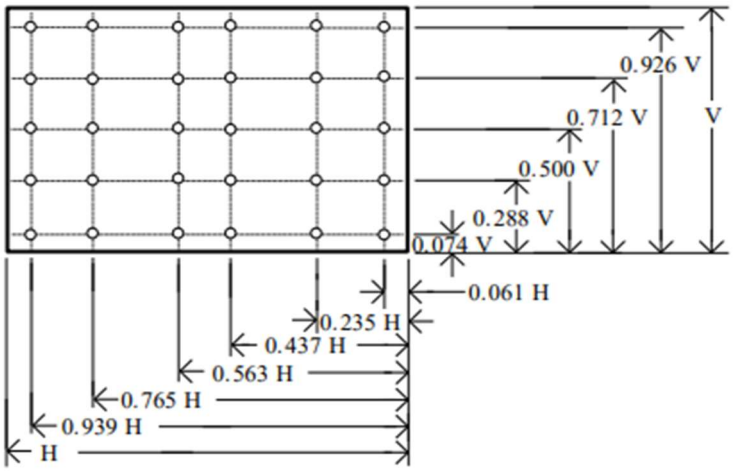

Figure 9. Velocity measurement schema

The number of data points were taken along each side of the duct depending on the side size of the duct. The distance to the points applied according to (TSI Instruments Ltd, 2014). The Testo-425 anemometer was used for velocity measurement. Instead of a pitot tube, an air velocity sensor was used for better accuracy and repeatability (Damiano, 2009). Calibration processes with pitot tube have a limitation that might be presented during the measurement. The main limitation is the relatively high measurement error in a low velocity flow (Benson, 2018). The main advantage of the velocity sensor over the pitot tube is that the velocity sensor has a lower angle sensitivity compared to the pitot tube. The angle between the flow and the instrument has less impact to the velocity sensor than to the pitot tube.

3.3.2 Calibration process realization

The air blower was supplied with an analog motor controller. Twenty steps of voltage input to the motor was selected to calibrate the tested sensor with the velocity sensor. A power range from 0 W to 51 W was selected. The results are illustrated in Table 1.

Table 1. Calibration data

Power W	Output signal from bypass sensor +\- 0.01V	Main channel velocity average from 25 points, 2 experiment m/s
0.0	0.525	0
3.7	0.784	1.23
5.8	0.995	1.73
8.3	1.246	2.3
11.0	1.464	2.9
14.2	1.625	3.52
17.9	1.778	4.07
21.9	1.914	4.65
25.7	2.058	5.58
29.5	2.162	6.25
33.2	2.247	7.09
35.7	2.317	7.93
38.3	2.377	8.44
40.8	2.414	9.05
43.4	2.444	9.3
45.9	2.470	9.7
48.5	2.480	9.8
51.0	2.503	9.96

Power W	Output signal from bypass sensor +\- 0.01V	Main channel velocity average from 25 points, 1 experiment m/s
0.0	0.525	0
3.7	0.765	1.21
5.8	0.980	1.69
8.3	1.240	2.49
11.0	1.433	2.93
14.2	1.573	3.67
17.9	1.769	4.31
21.9	1.896	4.9
25.7	2.049	5.64
29.5	2.158	6.75
33.2	2.251	7.41
35.7	2.338	8.09
38.3	2.386	8.74
40.8	2.416	9.14
43.4	2.444	9.37
45.9	2.467	9.85
48.5	2.483	10.09
51.0	2.497	10.18

Power W	Output signal from bypass sensor +\- 0.01V	Main channel velocity average from 25 points, 2th experiment m/s
0.0	0.525	0.00
3.7	0.76	1.18
5.8	0.986	1.81
8.3	1.230	2.20
11.0	1.453	2.95
14.2	1.645	3.47
17.9	1.783	4.14
21.9	1.918	4.83
25.7	2.051	5.42
29.5	2.170	6.34
33.2	2.246	7.13
35.7	2.326	7.86
38.3	2.388	8.63
40.8	2.422	9.21
43.4	2.445	9.41
45.9	2.466	9.74
48.5	2.485	9.81
51.0	2.496	10.07

The output voltage from the sensor was measured by FLUKE 175 True RMS multimeter. The measurement process of the airflow velocity and calibration was as follow:

The air blower speed controller was set according to the preinstalled modes, first at 3.7 W and then up to 51 W (maximum power that could be supplied by the laboratory stand). 18 modes were tested in total.

The anemometer was set to the sample-based average mode.
Samples were taken from each measuring point, leading to 30 samples per mode, and a total of 540 measurement points were taken during one experiment.

The measurement was repeated three times to determine the error margin of the experiment. The total number of measurements taken was 1620. The results shown in Table 1.

The averaged values from the three experiments were used to find the total airflow velocity in the main duct for each blower mode. The Excel program was used to calculate the average value.

The bypass sensor's output was read with a Fluke 175 multimeter during the complete experiment to find out a connection between the airflow in the main channel and the sensor's output. The voltage output of the sensor was checked in an "average" setting of the multimeter during the experiment. All the settings were set according to the recommendation in the manual (Fluke users manual models 175, 177, 179, 2003)

3.4 **Determination of mathematical function**

3.4.1 Nonlinear regression modeling

In order to determine the relation between the bypass sensor output and the actual volumetric flow rate in the main channel, a regression analysis of these two variables was conducted, following the recommendations from Young, (2019) as described in chapter 2.2 in this thesis. Excel was used to ensure the correctness of the calculations following the method described in the article Young, (2019). The final model is illustrated in Fig 10. The values of the sensor's output and the calculated volumetric air flow Q in liters per second were plotted on an Excel sheet. The plot with x-axis was Q in l/s and the y-axis was the sensor's output in Volts. The Excel sheet with its values is here as Appendix 1.

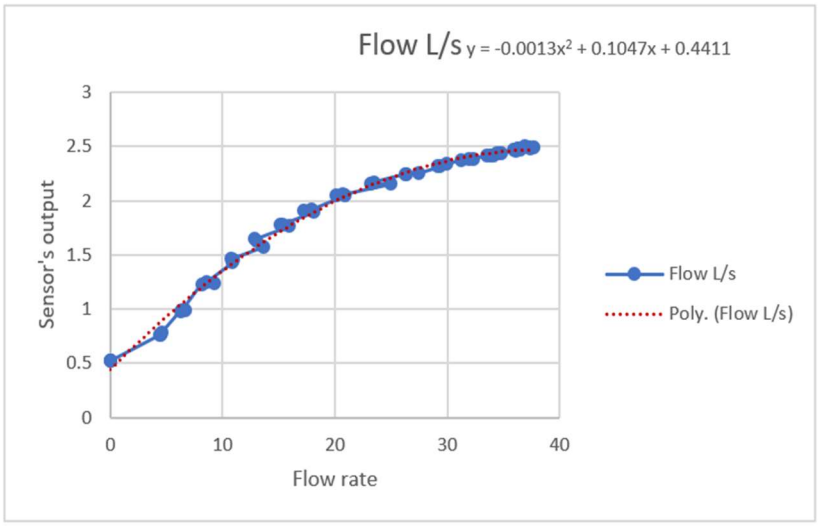

Figure 1 Regression fitting model

The sensor output value as function of the flow yields equation 9

$$V_s = -0.0013Q^2 + 0.1047Q + 0.4411 \quad (9)$$

Where:
V_s : sensor's output in V;
Q: volume flow rate in l/s;

The graph in Figure 9 with the blue line and dots illustrates the connection between the measured flow rate values and the measured sensor output. The red-dotted line is an illustration of a second-degree polynomial function. The red-dotted line is the regression model of the blue-dotted line. Equation 9 represents the modeled flow sensor's output values as a function of the flow in the air duct.

Graphically we can see that the blue and red-dotted lines plotted into the same scale are nearly identical. It gives us a visual confirmation of the connection between the two graphs. The result of the regression modeling is a second-degree polynomial, illustrated in equation 9. Low absolute values of polynomial coefficient show that the sensor has a relatively high resolution across the complete measured range. In other words, the slightest changes in the flow will be detected and measured by the sensor. Overall, the graph in Fig 10 and equation 9 testify that the regression model of the voltage output represents a connection between the sensor output and the flow in the duct. The quality of the regression model itself is evaluated in chapter 3.4.2.

3.4.2 Analysis of the regression model

In order to verify the correctness of the regression model, a residuals analysis was made as described in chapter 2.2. The residual plot is illustrated in Fig 11. It is clear from the plot, that the second-degree polynomial form at equation 9 is generally a suitably fitting method for describing the relationship between the flow in the duct and the sensor output, and that it can be used for control application. The residuals are rather randomly presented on the plot in a range between the -0.15 and 0.1.

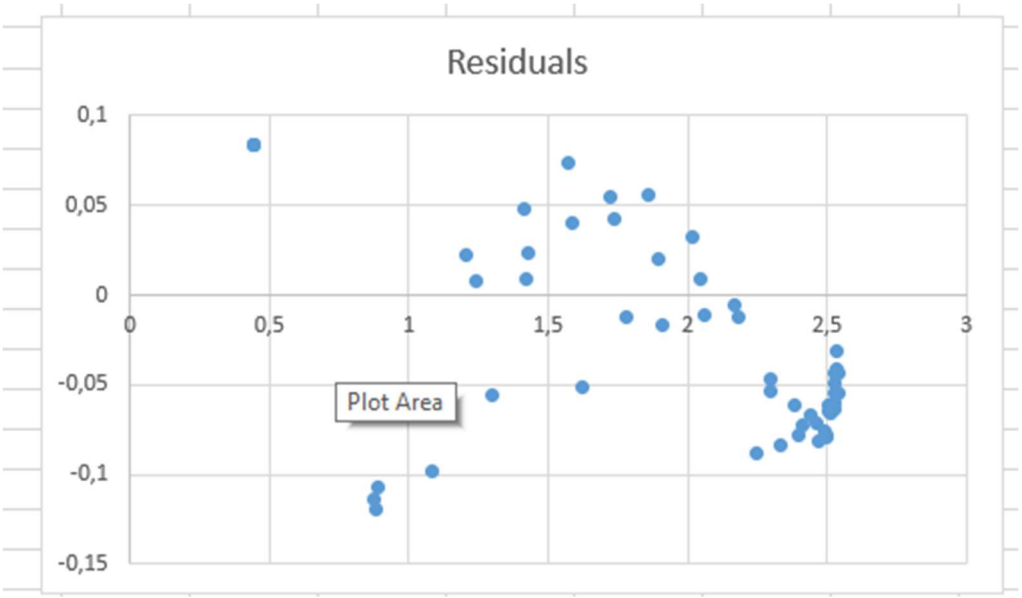

Figure 10. Residuals plot

Whiteness test criteria described section 2.2 of this thesis is generally met by the function. It is also clear that residuals are overrepresented on the right side of the plot. This is because there were more measurements made between 2 and 2.5 V. Additional testing is needed for this specific range. A detailed plot was made in the 2-2.5 V range and it is illustrated in the Fig 11. All the residuals are on the negative side but still above -0.1 and

the values are generally uncorrelated with the perverse inputs. The independence test criteria were met.

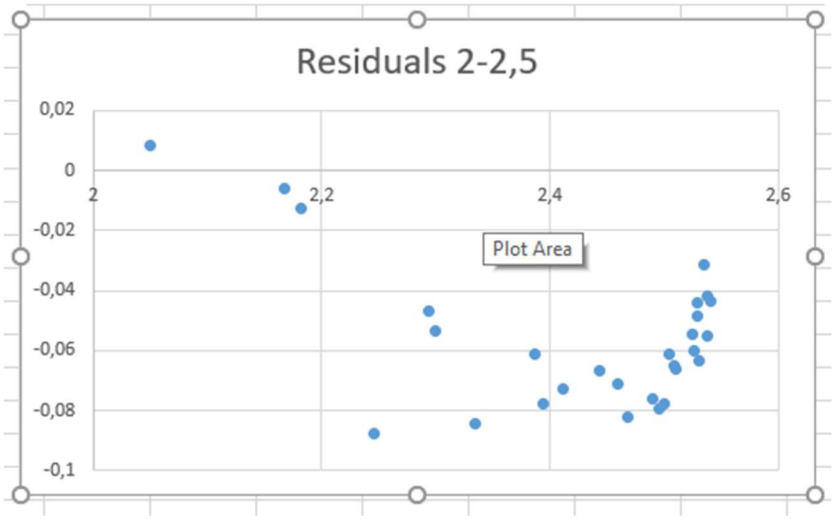

Figure 11. Residuals plot, range 2-2.5V

The least square test explained in chapter 2.2 was made with Excel and the results are presented in table 2. The interpretation criteria were according to Hargreaves, Croft, Davison, & Flint, (2012) and Ablebits' database web site, according to Cheusheva, (2019)

Table 2. Regression statistics

Regression Statistics	
Multiple R	0,972602223
R Square	0,945955084
Adjusted R Square	0,944915759
Standard Error	0,151867723
Observations	54

The R-square value was calculated from the total sum of squares, more precisely, it was the sum of the squared deviations of the original data from the mean. The value manifests a strong relationship between the flow in the main duct and the sensors' modeled values.

4 ERROR EVALUATION AND DISCUSSION

Error evaluation is needed in order to understand the performance of the designed system and the calculated mathematical function. Each dimension has the form of uncertainty, and not all uncertainties are equal. Therefore, the ability to correctly combine uncertainty with different dimensions is critical. Measurement uncertainty covers different types of equipment, such as different observers, differences in choice and time of

day. According to LibreTexts libraries and as a rule, the error is determined by the standard deviation of the measurement (Caldwell & Vahidsafa, 2019)

Known instrumentation error values:

- Fluke 175 DMM has 0.15 % + 2 deviation for resolution of 0.001 V (Fluke users manual models 175, 177, 179, 2003)
- D6f-ph0025ad1 sensor has ±0.10 V output voltage deviation. (MEMS Flow Sensors catalog, 2006)
- Testo-425 anemometer has ± (0.03 m/s +5 % of measured value) deviation for 0.01 m/s resolution (Data sheet Testo 425, 2018)

In chapter 4.4 it was described that in total three experiments were conducted. The measurements of velocity and flow sensors output were taken during three experiments and can be compared to find the deviation of the results. The standard deviation of the flow sensor measurements also included DMM deviations and those deviations were added to each measurement. The general form of the equation for addition of measured quantities is a special case of equation 7 and can be written in form of equation 10. (Caldwell & Vahidsafa, 2019)

$$\sigma_x = \sqrt{(\sigma_a^2 + \sigma_b^2 + \sigma_c^2)} \quad (10)$$

Where: σ - is the error value.
a, b, c -are the measured parameters

Substituting values from three experiments and combining them into Excel, the results are given in Table 3. The last column of the Table 3 includes average relative error values. Then total average relative error value was calculated to be +/- 6 %.

Table 3. Deviation for voltage output values

			Known deviation values %	+/- V	
		Fluke 175	0,15	0,002	
		D6f-ph0025ad1		0,100	
Output signal from bypass sensor Experiment 1 (V)	Output signal from bypass sensor Experiment 2 (V)	Output signal from bypass sensor Experiment 3 (V)	Standard Deviation V	Standard Deviation%	Adjusted average Standard Deviation %
0,525	0,525	0,525	0	0,000	0,0
0,765	0,76	0,784	0,013	1,6	13,1
0,980	0,986	0,995	0,008	0,8	10,2
1,240	1,230	1,246	0,008	0,7	8,1
1,433	1,453	1,464	0,016	1,1	7,0
1,573	1,645	1,625	0,037	2,3	6,6
1,769	1,783	1,778	0,007	0,4	5,6
1,896	1,918	1,914	0,012	0,6	5,3
2,049	2,051	2,058	0,005	0,2	4,9
2,158	2,170	2,162	0,006	0,3	4,6
2,251	2,246	2,247	0,003	0,1	4,5
2,338	2,326	2,317	0,011	0,5	4,3
2,386	2,388	2,377	0,006	0,2	4,2
2,416	2,422	2,414	0,004	0,2	4,1
2,444	2,445	2,444	0,001	0,0	4,1
2,467	2,466	2,470	0,002	0,1	4,1
2,483	2,485	2,480	0,003	0,1	4,0
2,497	2,496	2,503	0,004	0,2	4,0
			0,008	0,5	6

The measurement deviation for flow values was found with equation 10. Knowing the anemometer's error and by combining the values in the Table 4 one can calculate the average deviation of flow measurement. The value +/- 6% is calculated in the last column of Table 4.

Table 4. Deviation for flow measured values

			Known deviation values %	+/- m/s		
		Testo-425	5,00	0,030		
Step Of air blower	Main channel velocity average from 30 points, 1 experiment m/s	Main channel velocity average from 30 points, 2th experiment m/s	Main channel velocity average from 30 points, 3th experiment m/s	Standard Deviation m/s	Standard Deviation%	Adjusted average Standard Deviation %
1	0	0,00	0	0	0,00	0
2	1,21	1,18	1,23	0,025	2,09	5,96
3	1,69	1,81	1,73	0,061	3,50	6,34
4	2,49	2,20	2,3	0,147	6,32	8,16
5	2,93	2,95	2,9	0,025	0,86	5,18
6	3,67	3,47	3,52	0,104	2,93	5,86
7	4,31	4,14	4,07	0,123	2,96	5,85
8	4,9	4,83	4,65	0,129	2,69	5,71
9	5,64	5,42	5,58	0,114	2,05	5,43
10	6,75	6,34	6,25	0,267	4,13	6,50
11	7,41	7,13	7,09	0,174	2,42	5,57
12	8,09	7,86	7,93	0,118	1,48	5,23
13	8,74	8,63	8,44	0,152	1,76	5,31
14	9,14	9,21	9,05	0,080	0,88	5,09
15	9,37	9,41	9,3	0,056	0,59	5,05
16	9,85	9,74	9,7	0,078	0,80	5,07
17	10,09	9,81	9,8	0,165	1,66	5,28
18	10,18	10,07	9,96	0,110	1,09	5,13
Average				0,113	2,25	6

When rewriting equation 9 and isolating Q, it is now possible to determine the volumetric flow value in the main channel based on the flow sensor

output. Equation 11 is the volume flow rate value in l/s as the function of the sensor's output in volts.

$$Q = -\frac{\sqrt{-520000 * V + 1235581} + 1047}{26} \quad (11)$$

Where:
V_s: sensor's output in V;
Q: volume flow rate in l/s;

Evaluating the error of the flow rate we used the derivative method described in chapter 2.3. We know that Q= A*V, where A – area of the duct and V – velocity. A is the calculated value from the drawing dimensions. The duct was 3D printed with 0.15 mm resolution, so it is +/- 0.3 mm (0.0003m) error range for wall thickness. Area was calculated with equation 12:

$$A = a * b$$
$$a = 83.6mm(0.0836m); b = 44.3mm(0.0443m) \quad (12)$$
$$A = 0{,}003703\ m\text{^}2.$$

According to a formula for arithmetic calculations of error propagation (Caldwell & Vahidsafa, 2019), the error for area was defined by equation 13.

$$\frac{\sigma_x}{x} = \sqrt{\left(\frac{\sigma_a}{a}\right)^2 + \left(\frac{\sigma_b}{b}\right)^2 + \left(\frac{\sigma_c}{c}\right)^2} \quad (13)$$

$$\frac{\sigma_A}{A} = \sqrt{\left(\frac{0.0003}{0.0836}\right)^2 + \left(\frac{0.0003}{0.0443}\right)^2} \approx 0.0076 \approx 0.8\%$$

The error of V is +/-0.12 m/s. The error for the volume flow rate was calculated with equation 7 from chapter 2.3 and yields equation 14.

$$Q = A * V$$

$$\frac{dQ}{dA} = V\ ; \frac{dQ}{dV} = A \quad (14)$$

$$dQ = V * dA + A * dV = V * 0.8A + A*6V = 6.8AV$$

The error of the volume flow rate values is +/- 7 % when a modeled equation is used for the programming application.

5 CONCLUSION AND RECOMMENDATIONS

The goal of this thesis project was to design, calibrate, test and implement an air flow measurement solution for a pellet burning water heater. The designed sensor extension combined with a calibrated instrument and a mathematical function proved to be a good alternative to expensive measuring factory-grade instrumentation. The total cost of the instrument and the printed extension was approximately 70 euros including the sensor and the 3D printing material. The designed extension was installed and tested on the VEneCT project site at HAMK's Valkeakoski campus. The described methods introduce a cost-efficient method for collecting data from small-scale processes in general.

The accuracy of the measurement is acceptable but can be improved in the future with a better-quality sensor. A printed extension can be replaced in the future with a CNC manufactured part for lower manufacturing errors. Steel or aluminium are recommended instead of plastic for longevity of the physical parts.

The 3D printed sensor's mounting point was installed to the process and used to collect the flow parameters in multiple real-life process operations. The installed extension is illustrated in Fig 12.

Figure 12. Installed solution

The relatively low total average error of flow measurement (7 %) makes it possible to collect reliable flow rate information and use the data for a future optimization of the combustion process. Multiple calibration experiments have proven that the sensor mounting extension provides a good quality air flow that can be measured with MEMS or potentially any other sensor type.

CFD simulating of the flow process helped to minimize the time consuming and costly prototyping and testing stages. Nowadays, CFD software is available to small manufacturers and private users. Easy access to the CFD software and 3D printing creates potential for further implementation of the results of this thesis project for similar applications. Testing and optimization with the CFD design increased the overall quality of the final sensor extension and the collected data. The simulation made it possible to design a suitable solution with the resources available. Based on the results, it was possible to design the air restrictor significantly smaller than it would have been with more traditional methods.

This research and development project demonstrate that the measurement of the air flow in small-scale alternative energy and heat stations can be accomplished with MEMS, avoiding the high cost of industry level sensors.

REFERENCES

Benson, T. (2018). *Pitot tubes*. Retrieved June 05, 2019, from NASA web page: https://www.grc.nasa.gov/WWW/k-12/VirtualAero/BottleRocket/airplane/pitot.html

Caldwell, J., & Vahidsafa, A. (2019). *Propagation of Error*. Retrieved September 30, 2019, from LibreTexts: https://chem.libretexts.org/Bookshelves/Analytical_Chemistry/Supplemental_Modules_(Analytical_Chemistry)/Quantifying_Nature/Significant_Digits/Propagation_of_Error

Cheusheva, S. (2019). *Linear regression analysis in Excel*. Retrieved November 26, 2019, from AbleBits corporate site: https://www.ablebits.com/office-addins-blog/2018/08/01/linear-regression-analysis-excel/

Dahad, N., & Pele, A.-F. (2019). *10 Highlights at MEMS & Imaging Sensors Summit*. Retrieved November 20, 2019, from Aspencore web site: https://www.eetimes.com/document.asp?doc_id=1335159&page_number=2#

Damiano, L. A. (2009). *Sources of differences between expected and actual performance.* Retrieved November 30, 2019, from HPAC ENGINEERING web site: https://www.hpac.com/archive/article/20925400/evaluating-airflowmeasuring-devices

Gruener, W., & Miconi, C. (2018). *Intel Processors Over the Years*. Retrieved December 13, 2019, from Businessnewsdaily web site: https://www.businessnewsdaily.com/10817-slideshow-intel-processors-over-the-years.html

Hargreaves, M., Croft, A., Davison, R., & Flint, J. (2012). Engineering Mathematics. In *A foundation for electronic, electrical, communications and systems engineers* (pp. 891-934). Pearson Education M.U.A. Retrieved September 30, 2019

Young, C. (2019). *Nonlinear curve fitting in excel*. Retrieved December 05, 2019, from High Creek Commerce, LLC EngineerExcel.com: https://www.engineerexcel.com/nonlinear-curve-fitting-in-excel/

Data sheet Testo 425. (2018). Retrieved January 20, 2020, from Testo corporate web page: https://static-int.testo.com/media/ef/2e/e09ea9551de8/testo-425-Data-sheet.pdf

ISO 3966:2008 Measurement of fluid flow in closed conduits. (2008). Retrieved January 20, 2020, from International Organization for Standardization: https://www.iso.org/standard/50626.html

ISO 5167-4:2003 Measurement of fluid flow by means of pressure differential devices inserted in circular cross-section conduits running full — Part 4: Venturi tubes. (2003). Retrieved December 20, 2019, from International Organization for Standardization site: https://www.iso.org/standard/30192.html

Fluke users manual models 175, 177, 179. (2003). Retrieved November 20, 2019, from Fluke Corporation web site: http://assets.fluke.com/manuals/175_____umeng0000.pdf

MEMS Flow Sensors catalog. (2006). Retrieved December 01, 2019, from Omron corporate web page: https://omronfs.omron.com/en_US/ecb/products/pdf/en-d6f_series.pdf

Sensors Selector Guide. (2018). Retrieved December 20, 2019, from Omron corporate site: https://omronfs.omron.com/en_US/ecb/products/pdf/en_Y232-E1.pdf

TSI Instruments Ltd. (2014). *Traversing a duct to determine average air velocity or volume.* Retrieved December 15, 2019, from TSI Instruments Ltd Incorporated web site: https://www.tsi.com/getmedia/1a11d344-0a58-4ca6-94fe-65721825686b/AF-106%20Traversing%20a%20Duct?ext=.pdf

What Is Residual Analysis? (n.d.). Retrieved December 20, 2019, from MathWorks, Inc. corporate web site: https://se.mathworks.com/help/ident/ug/what-is-residual-analysis.html

APPENDICES

Appendix 1

Function evaluation sheet

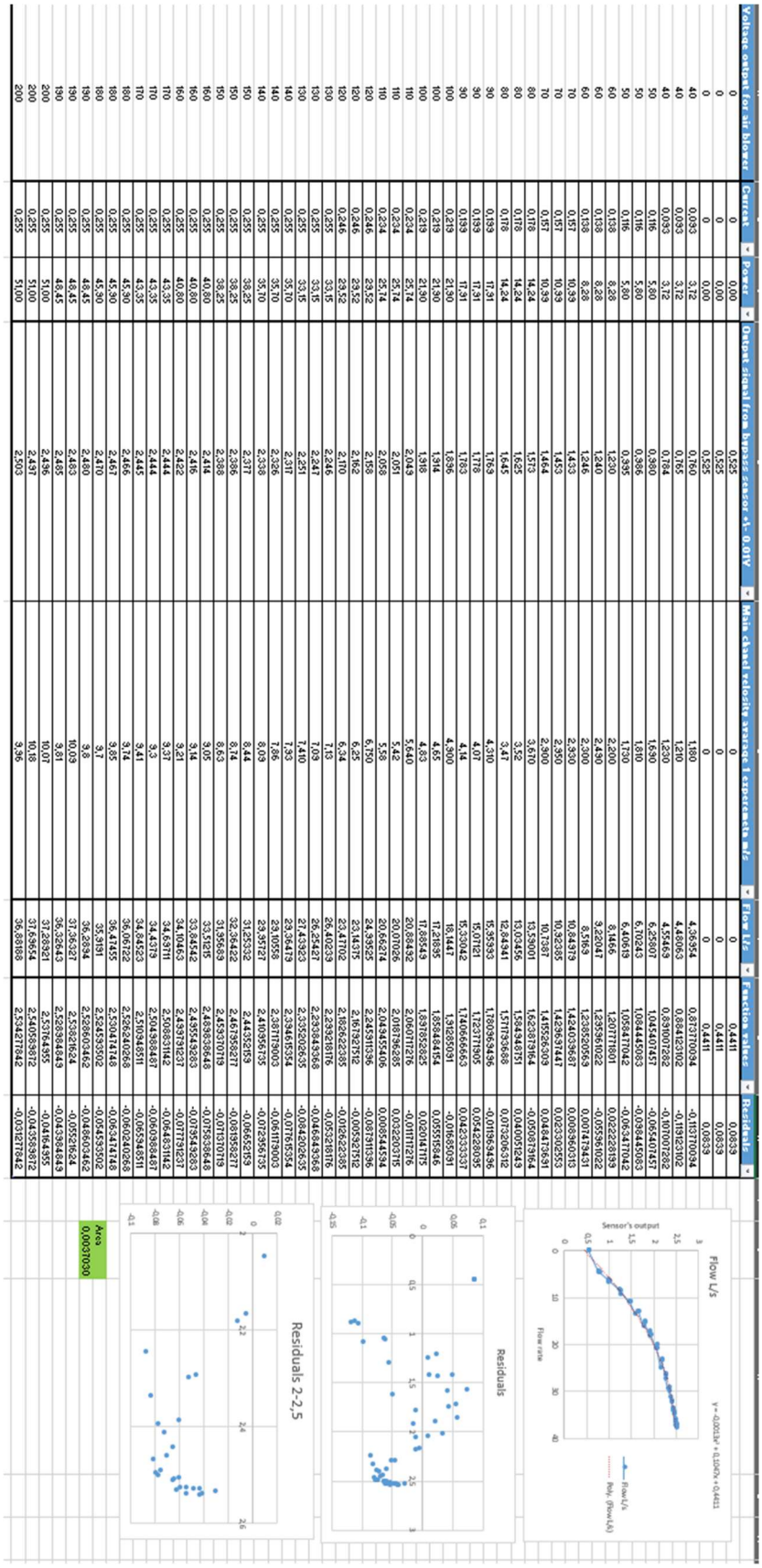

Voltage output for air blower	Current	Power	Output signal from bypass sensor +/- 0.01V	Main chanel velocity average 3 experiments m/s	Flow L/s	Function values	Residuals
0	0	0,00	0,525	0	0	0,4411	0,0839
0	0	0,00	0,525	0	0	0,4411	0,0839
0	0	0,00	0,525	0	0	0,4411	0,0839
40	0,093	3,72	0,760	1,690	4,326954	0,871170934	-0,193170934
40	0,093	3,72	0,765	1,270	4,48063	0,884182902	-0,191382902
40	0,093	3,72	0,784	1,230	4,53463	0,891001282	-0,197001282
50	0,116	5,80	0,360	1,690	6,25901	1,045401451	-0,045401451
50	0,116	5,80	0,366	1,810	6,70243	1,098445083	-0,098445083
50	0,116	5,80	0,395	1,730	6,40619	1,058417042	-0,058417042
60	0,138	8,28	1,230	2,200	8,1466	1,207771601	0,022228399
60	0,138	8,28	1,240	2,490	9,22047	1,295961022	-0,055961022
60	0,138	8,28	1,246	2,300	8,5163	1,238520569	0,001479431
70	0,157	10,99	1,433	2,930	10,84979	1,424039687	0,008960313
70	0,157	10,99	1,453	2,950	10,92385	1,429637447	0,023302553
70	0,157	10,99	1,464	2,900	10,7387	1,415526309	0,048473691
80	0,178	14,24	1,573	3,670	13,59001	1,562387964	-0,050387964
80	0,178	14,24	1,625	3,52	13,03456	1,504349751	0,040050249
80	0,178	14,24	1,645	3,47	12,84341	1,571739688	0,073260312
90	0,193	17,31	1,763	4,310	15,95393	1,780963496	-0,011963496
90	0,193	17,31	1,778	4,07	15,07121	1,723771905	0,054228095
90	0,193	17,31	1,783	4,14	15,33042	1,740666663	0,042333337
100	0,213	21,30	1,896	4,900	18,1447	1,918265031	-0,016265031
100	0,213	21,30	1,914	4,65	17,21695	1,858484154	0,055515846
100	0,213	21,30	1,916	4,83	17,88543	1,901852625	0,012047375
110	0,234	25,74	2,043	5,640	20,88432	2,086117216	-0,011117216
110	0,234	25,74	2,051	5,42	20,07026	2,038796285	0,035203715
110	0,234	25,74	2,058	5,58	20,66214	2,043455406	0,030544594
120	0,246	29,52	2,158	6,750	24,99525	2,245911396	-0,087911396
120	0,246	29,52	2,162	6,25	23,14375	2,136792192	-0,005792192
120	0,246	29,52	2,170	6,34	23,47702	2,156622385	-0,025622385
130	0,255	33,15	2,246	7,13	26,40239	2,329218176	-0,052218176
130	0,255	33,15	2,247	7,09	26,25427	2,320843568	-0,043843568
130	0,255	33,15	2,251	7,410	27,43923	2,335820635	-0,058820635
140	0,255	35,70	2,317	7,93	29,36479	2,394615354	-0,017615354
140	0,255	35,70	2,326	7,86	29,10558	2,381179003	-0,004179003
140	0,255	35,70	2,338	8,09	29,95727	2,440956735	-0,072956735
150	0,255	38,25	2,377	8,44	31,25332	2,44352159	-0,06652159
150	0,255	38,25	2,386	8,14	30,16422	2,467958277	-0,091958277
150	0,255	38,25	2,388	8,63	31,95583	2,453370719	-0,077370719
160	0,255	40,80	2,414	9,05	33,51215	2,489393648	-0,075393648
160	0,255	40,80	2,416	8,74	32,36442	2,435543283	-0,021543283
160	0,255	40,80	2,422	8,81	32,64542	2,453751237	-0,039751237
170	0,255	43,35	2,444	9,37	34,70463	2,580631142	-0,067631142
170	0,255	43,35	2,444	9,3	34,4379	2,564368487	-0,051368487
170	0,255	43,35	2,445	9,41	34,84523	2,59104511	-0,07604511
180	0,255	45,90	2,466	9,74	36,06722	2,526240268	-0,040240268
180	0,255	45,90	2,467	9,65	36,47455	2,550414748	-0,064414748
180	0,255	45,90	2,470	9,7	35,9191	2,524593502	-0,038593502
190	0,255	48,45	2,480	9,8	36,2894	2,528603462	-0,042603462
190	0,255	48,45	2,483	10,03	37,26327	2,53821624	-0,05521624
190	0,255	48,45	2,485	9,81	36,32643	2,528384849	-0,043384849
200	0,255	51,00	2,496	10,07	37,28921	2,57364955	-0,04164955
200	0,255	51,00	2,497	10,18	37,69654	2,540589872	-0,004589872
200	0,255	51,00	2,503	9,96	36,88188	2,534277842	-0,033277842

Appendix 2

Experiment log book

Voltage output for air blower +/- 0.5V	Current output for air blower	Power W	Output signal from bypass sensor +/- 0.01V	Main chanel velocity average from 25 points, 1 experiments m/s
0,0	A	0,0	0,525	0
40,0	0,0353	3,7	0,765	1,21
50,0	0,116	5,8	0,980	1,69
60,0	0,158	8,3	1,240	2,49
70,0	0,157	11,0	1,453	2,93
80,0	0,178	14,2	1,573	3,67
90,0	0,193	17,3	1,763	4,31
100,0	0,219	21,9	1,936	4,9
110,0	0,234	25,7	2,049	5,64
120,0	0,246	29,5	2,156	6,15
130,0	0,255	33,2	2,251	7,41
140,0	0,255	35,7	2,338	8,09
150,0	0,255	38,3	2,396	8,74
160,0	0,255	40,8	2,416	9,14
170,0	0,255	43,4	2,444	9,37
180,0	0,255	45,9	2,461	9,85
190,0	0,255	48,5	2,463	10,09
200,0	0,255	51,0	2,431	10,18

Experiment 2, T= 296,15 K						
Voltage output for air blower +/- 0.5V	Current output for air blower	Power W	Output signal from bypass sensor +/- 0.01V	Main chanel velocity average from 25 points, 2th experiment	AREA m^2	Air Flow U/s
0,0	A	0,0	0,525	0,00	0,0037030	m^3/h
40,0	0,0353	3,7	0,765	1,61		0
50,0	0,116	5,8	0,985	1,91	0,0044364	15,730344
60,0	0,158	8,3	1,230	2,20	0,0067043	24,128148
70,0	0,157	11,0	1,453	2,95	0,0089660	33,32776
80,0	0,178	14,2	1,645	3,47	0,0109385	41,03586
90,0	0,193	17,3	1,783	4,14	0,0126434	46,257876
100,0	0,219	21,9	1,916	4,83	0,0141868	53,02586
110,0	0,234	25,7	2,051	5,42	0,0157549	55,185512
120,0	0,246	29,5	2,170	6,24	0,0172470	64,397764
130,0	0,255	33,2	2,246	7,13	0,0185723	72,252936
140,0	0,255	35,7	2,326	7,86	0,0199560	84,571272
150,0	0,255	38,3	2,388	8,63	0,0210558	95,048604
160,0	0,255	40,8	2,422	9,21	0,0219463	104,780088
170,0	0,255	43,4	2,445	9,41	0,0224523	115,044804
180,0	0,255	45,9	2,456	9,74	0,0230607	122,776668
190,0	0,255	48,5	2,485	9,81	0,0236264	125,442828
200,0	0,255	51,0	2,496	10,07	0,0237839	130,71546

Experiment 3, T= 294,5 K					
Voltage output for air blower	Current output for air blower	Power W	Output signal from bypass sensor +/- 0.01V	Main chanel velocity average from 25 points, 2 experiments m/s	
0	A	0,0	0	0	
40	0,0353	3,7	0,764	1,23	
50	0,116	5,8	0,955	1,73	
60	0,158	8,3	1,245	2,3	
70	0,157	11,0	1,454	2,93	
80	0,178	14,2	1,578	3,52	
90	0,193	17,3	1,768	4,07	
100	0,219	21,9	1,914	4,65	
110	0,244	25,7	2,059	5,58	
120	0,246	29,5	2,162	6,25	
130	0,255	33,2	2,247	7,09	
140	0,255	35,7	2,317	7,93	
150	0,255	38,3	2,377	8,44	
160	0,255	40,8	2,414	9,05	
170	0,255	43,4	2,444	9,3	
180	0,255	45,9	2,470	9,7	
190	0,255	48,5	2,480	9,8	
200	0,255	51,0	2,503	9,96	

Appendix 3

Error evaluation log

				Known deviation values %	+/- V	
			Fluke 175	0,15	0,002	
			D6f-ph0025ad1		0,100	
Step Of air blower	Output signal from bypass sensor Experiment 1 (V)	Output signal from bypass sensor Experiment 2 (V)	Output signal from bypass sensor Experiment 3 (V)	Standard Deviation V	Standard Deviation %	Adjusted average Standard Deviation %
1	0,525	0,525	0,525	0	0,000	0,0
2	0,765	0,76	0,784	0,013	1,6	13,1
3	0,980	0,986	0,995	0,008	0,8	10,2
4	1,240	1,230	1,246	0,008	0,7	8,1
5	1,433	1,453	1,464	0,016	1,1	7,0
6	1,573	1,645	1,625	0,037	2,3	6,6
7	1,769	1,783	1,778	0,007	0,4	5,6
8	1,896	1,918	1,914	0,012	0,6	5,3
9	2,049	2,051	2,058	0,005	0,2	4,9
10	2,158	2,170	2,162	0,006	0,3	4,6
11	2,251	2,246	2,247	0,003	0,1	4,5
12	2,338	2,326	2,317	0,011	0,5	4,3
13	2,386	2,388	2,377	0,006	0,2	4,2
14	2,416	2,422	2,414	0,004	0,2	4,1
15	2,444	2,445	2,444	0,001	0,0	4,1
16	2,467	2,466	2,470	0,002	0,1	4,1
17	2,483	2,485	2,480	0,003	0,1	4,0
18	2,497	2,496	2,503	0,004	0,2	4,0
Average				0,008	0,5	6

			Known deviation values %	+/- m/s		
		Testo-425	5,00	0,030		
Step Of air blower	Main channel velocity average from 30 points, 1 experiment m/s	Main channel velocity average from 30 points, 2th experiment m/s	Main channel velocity average from 30 points, 3th experiment m/s	Standard Deviation m/s	Standard Deviation%	Adjusted average Standard Deviation %
1	0	0,00	0	0	0,00	0
2	1,21	1,18	1,23	0,025	2,09	5,96
3	1,69	1,81	1,73	0,061	3,50	6,34
4	2,49	2,20	2,3	0,147	6,32	8,16
5	2,93	2,95	2,9	0,025	0,86	5,18
6	3,67	3,47	3,52	0,104	2,93	5,86
7	4,31	4,14	4,07	0,123	2,96	5,85
8	4,9	4,83	4,65	0,129	2,69	5,71
9	5,64	5,42	5,58	0,114	2,05	5,43
10	6,75	6,34	6,25	0,267	4,13	6,50
11	7,41	7,13	7,09	0,174	2,42	5,57
12	8,09	7,86	7,93	0,118	1,48	5,23
13	8,74	8,63	8,44	0,152	1,76	5,31
14	9,14	9,21	9,05	0,080	0,88	5,09
15	9,37	9,41	9,3	0,056	0,59	5,05
16	9,85	9,74	9,7	0,078	0,80	5,07
17	10,09	9,81	9,8	0,165	1,66	5,28
18	10,18	10,07	9,96	0,110	1,09	5,13
Average				0,113	2,25	6